Tetrahedron 68 (2012) 10351–10359

Contents lists available at SciVerse ScienceDirect

Tetrahedron

journal homepage: www.elsevier.com/locate/tet

Cubic nonlinear optical properties of new zinc tetraphenyl porphyrins peripherally functionalized with electron-rich Ru(II) alkynyl substituents

Samuel Drouet [a], Areej Merhi [b], Dandan Yao [b], Marie P. Cifuentes [c], Mark G. Humphrey [c,*], Malgorzata Wielgus [d], Joanna Olesiak-Banska [d], Katarzyna Matczyszyn [d], Marek Samoc [d,e,*], Frédéric Paul [a,*], Christine O. Paul-Roth [a,b,*]

[a] Institut des Sciences Chimiques de Rennes, ISCR-UMR CNRS 6226, Université de Rennes 1, Campus de Beaulieu, 35042 Rennes Cedex, France
[b] INSA-ISCR-UMR 6226, Université Européenne de Bretagne, INSA de Rennes, 35043 Rennes Cedex, France
[c] Research School of Chemistry, Australian National University, Canberra ACT 0200, Australia
[d] Institute of Physical and Theoretical Chemistry, Wroclaw University of Technology, 50-370 Wroclaw, Poland
[e] Laser Physics Centre, Australian National University, Canberra ACT 0200, Australia

ARTICLE INFO

Article history:
Received 9 July 2012
Received in revised form
24 September 2012
Accepted 25 September 2012
Available online 29 September 2012

Keywords:
Porphyrin
Acetylide complex
Organometallics
Nonlinear optics
Pi-conjugation

ABSTRACT

We report the synthesis and characterization of new organometallic assemblies consisting of a central Zn(II) tetraphenylporphyrin (ZnTPP) core surrounded by four Ru(II) alkynyl complexes (*trans*-Ru(dppe)$_2$R) appended at the *para* phenyl positions and acting as peripheral donor groups. The synthesis of the tetra-chlorido derivative **2** (R=Cl) is reported first, followed by that of three extended homologues (**3**–X) obtained from this building block by substitution of the chlorido ligands by functionalized arylacetylenes (R=C≡C(4-C$_6$H$_4$X); X=NO$_2$, H, OMe). Measurement of the nonlinear absorption properties of the pentametallic derivatives **3**–X reveals that these extended π-networks incorporating polarizable organometallic units behave as good two-photon absorbers in the visible and near-IR range.

1. Introduction

Materials with cubic nonlinear optical (NLO) properties are required in emerging photonics-based technologies for various applications, including optical data storage, nanophotonics, and biophotonics.[1,2] The processing of optical signals such as ultrafast switching or modulation of optical beams using materials with sizeable third-order NLO responses is of significant interest.[3] Amongst the wide range of molecular chromophores investigated in the last 30 years, organometallic and coordination compounds have emerged as very promising building blocks to access new NLO-active materials.[4,5] In particular, several examples of formally alkynyl-d^6 complexes featuring an equatorial 'Ru(dppe)$_2$' core [dppe=1,2-bis(diphenylphosphino)ethane] have been explored.[5,6] When such polarizable units are incorporated into extended π networks, a tremendous enhancement of the nonlinear optical response was often observed.[6,7] In the pursuit of optimized systems, these organometallic units permit great structural control, as the diphosphines coordinating the metal centre, the oxidation state of the metal, and the ligand trans to the alkynyl ligand can all be varied at will. Moreover, due to the existence of kinetically stable oxidized state(s) with distinct NLO properties at selected wavelengths, redox-switching of the NLO behaviour has been demonstrated in several instances with these particular building blocks.[8,9]

On another front, large metallated π-compounds such as porphyrins or phthalocyanines were also identified very early as efficient and robust cubic NLO-phores.[10–12] For instance, Rao et al. showed in 2000 that various metallated tetra-*p*-tolylporphyrins (TTP) could exhibit quite high cubic optical nonlinearities at 532 or 600 nm.[13] These properties were measured using nanosecond (and to a lesser degree picosecond) pulses, the results being consistent with contributions from mechanisms involving real excited states rather than virtual states only, as is the case with nonresonant cubic nonlinear responses, but rendering these molecules quite promising for optical limiting or all-optical switching purposes.[2] More recently, multi-porphyrin assemblies exhibiting enhanced cubic nonlinear absorption properties were also developed by various groups for related applications.[14,15] Thus, depending on the overall

* Corresponding authors. E-mail addresses: christine.paul@univ-rennes1.fr, christine.paul@insa-rennes.fr (C.O. Paul-Roth).

0040-4020/$ – see front matter © 2012 Elsevier Ltd. All rights reserved.
http://dx.doi.org/10.1016/j.tet.2012.09.108

symmetry of a given porphyrin, on the nature of the central metal ion, and on the peripheral substituents of the macrocyclic core, widely different nonlinearities can result. The presence of a metallic centre inside the porphyrin cavity usually proves to be crucial, since it planarizes the π-manifold, which is essential to achieve high hyperpolarizabilities.[11,12] Depending on its nature, the metal ion can also provide an additional electronic contribution to the NLO response. Accordingly, varying its nature is often a powerful way to optimize the cubic NLO response of a porphyrin-based chromophore tailored for a given application. In that respect, metal centres with low-lying charge-transfer states[16] or open-shell structures have often been usefully used.[11] In comparison, far fewer investigations have focused on the role of the peripheral substituents. However, among the scant experimental data available on metallated TPP derivatives, some investigations have suggested that electron-releasing substituents at the *para*-positions of the *meso*-aryl groups might afford higher cubic NLO activities.[11,17]

Some of us recently reported multistable alkynyl-d^6complexes exhibiting large and redox-switchable third-order (cubic) nonlinearities.[18] Others have reported the synthesis and properties of tetrafluorenyl porphyrin derivatives[19] and evidenced the determining role of the *meso*-substituents on the photophysical properties of these porphyrins.[20] However, to the best of our knowledge, only a few porphyrins featuring alkynyl metal complexes as peripheral substituents have been reported thus far,[21] with very few constructed around a TPP-core, such as in **1** (Scheme 1).[22] Moreover, none were studied from the perspective of their cubic NLO properties. We have consequently pursued the synthesis and third-order NLO responses of a series of new ZnTPP derivatives functionalized with electron-releasing alkynyl-d^6 Ru(II) complexes at the *para*-location of their *meso*-aryl groups.[23] By using the controlled stepwise reactivity of the *cis*-[$RuCl_2(dppe)_2$] and *trans*-Ru(C≡CAr)Cl($dppe)_2$] complexes,[24,25] derivatives with organoruthenium termini possessing differently functionalized terminal arylalkynyl ligands were targeted, in order to evidence the effect of electron-releasing or electron-attracting *para* substituents on their cubic NLO response. In this contribution, we report the stepwise synthesis and characterization of three new derivatives **3**–X (NO_2, H, OMe) via the corresponding tetra-chlorido precursor (**2**), followed by *Z*-scan measurements of their cubic nonlinear absorption properties.

itself obtained after metallation[27] of the corresponding tetra-alkyne free base, affords access to the pentametallic complex **2** (Scheme 2) in an overall yield of 32%. Although the tetra-alkyne Zn porphyrin **5** had been previously synthesized in fair yields (29%),[22] the present work (see Supplementary data) resulted in an improved yield (34% over 3 steps) by using the $BF_3(OEt_2)$ complex as a Lewis-acid promoter to assist the synthesis of the free base **1**.[28] The tetra-vinylidene complex that forms upon reaction of the Ru(II) precursor **4** with **5** by a 1,2-hydrogen shift was not characterized,[29] but was precipitated before being deprotonated in situ by excess triethylamine to give **2**. Completion of the reaction forming **2** can be monitored by following the disappearance of the ^{1}H NMR alkynyl proton (C≡CH) of **5** at 3.37 ppm in $CDCl_3$. This new complex was characterized by the usual spectroscopies (NMR, UV–vis and IR), microanalysis and electrospray mass spectrometry (ESI-MS).

In its ^{1}H NMR spectrum, **2** exhibits both the spectral signatures of the porphyrin core (a characteristic singlet at ca. 9 ppm, corresponding to the 8 equivalent β-pyrrolic protons) and signals typical of the σ-alkynyl Ru(II) endgroups, such as the broad singlet at ca. 3 ppm corresponding to the 32 equivalent CH_2 protons of the ruthenium-coordinated dppe. Between 6.5 and 9 ppm are the signals of the various aromatic protons of the porphyrin and of the dppe. The ^{31}P NMR spectrum of **2** reveals a sharp singlet corresponding to the 16 equivalent phosphorus atoms from the 8 dppe ligands coordinated to the ruthenium endgroups (Table 1); the chemical shift of this signal (ca. 50 ppm) is characteristic of monosubstituted σ-alkynyl ruthenium complexes of this kind.[30] Further evidence for the structure of this compound comes from the ^{13}C NMR spectrum, in which all carbon atoms of **2** can be observed and assigned by polarization transfer studies, except for the weak quintuplet corresponding to the C_α-alkyne carbon atoms, which escaped from detection. The presence of the four alkynyl bonds in **2** is nevertheless revealed by a broad singlet near 115 ppm, corresponding to the equivalent C_β carbon atoms.[25,31] The presence of these alkynyl bonds is more clearly revealed by infrared, since **2** displays an intense absorption band at ca. 2050 cm^{-1} (Table 1), characteristic of the $\nu_{C\equiv C}$ mode of these Ru(II) σ-alkynyl complexes.[25,30]

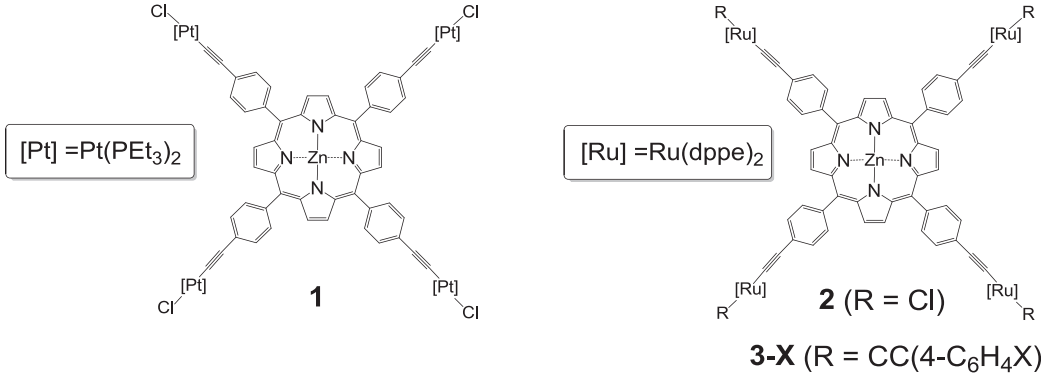

Scheme 1. Selected TPP-based porphyrins substituted with alkynyl complexes.

2. Results and discussion

2.1. Synthesis and characterization of the tetra(ruthenium-chloride) ZnTPP

Reacting the known *cis* ruthenium(II) organometallic precursor complex **4**[26] with the known tetra-alkyne zinc(II) porphyrin **5**,[22]

2.2. Synthesis and characterization of the tetra{ruthenium-bis(alkynyl)} Zn(II) porphyrins

Using the pentametallic porphyrin **2** as starting material, we have isolated three new derivatives **3**–X (X=NO_2, H, OMe) by ligand metathesis. This reaction was performed in the presence of sodium hexafluorophosphate and with an excess of the

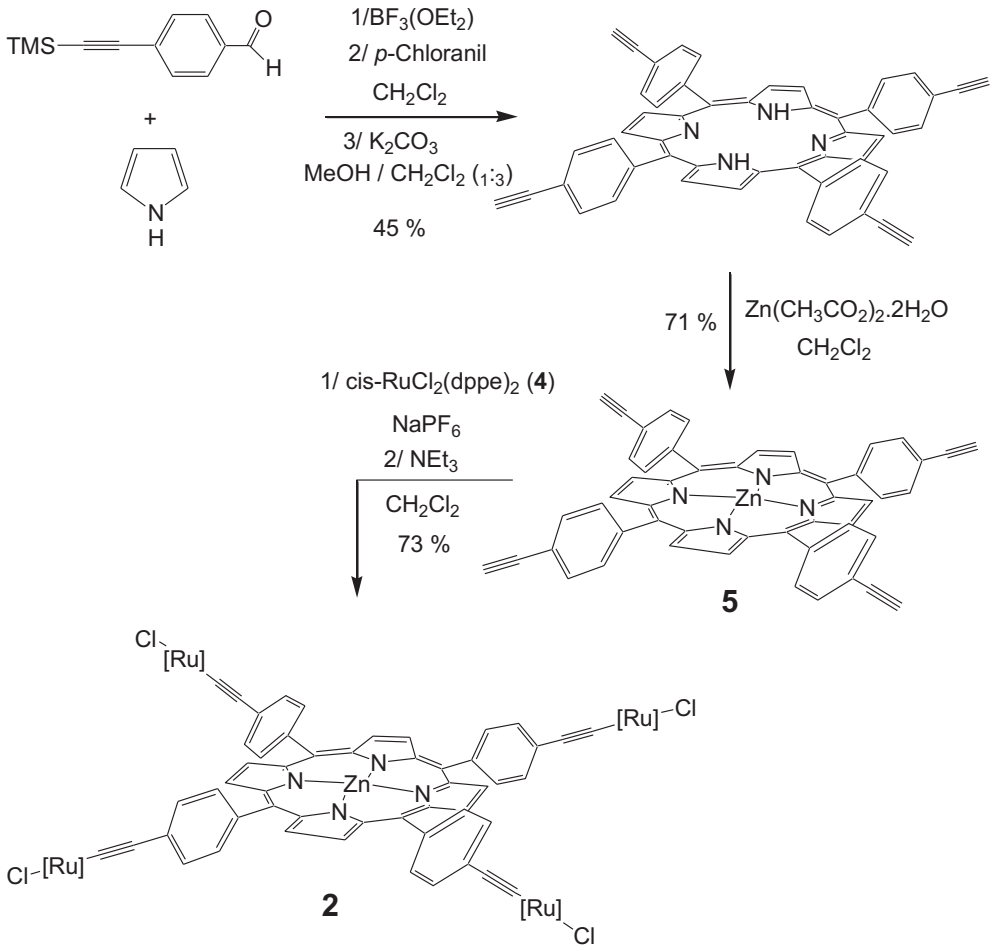

Scheme 2. Synthesis of the peripherally tetraruthenated ZnTPP porphyrin **2**.

Table 1
Selected spectral signatures for **2** and **3**–X complexes

Compounds	$\nu_{C\equiv C}$[a]	^{31}P NMR[b]
2	2057	51.0
3–NO_2	2042	54.7
3–H	2056	55.2
3–OMe	2056	55.1

[a] IR pellet in KBr.
[b] In $CDCl_3$.

corresponding functional arylethyne, using well-established reaction protocols developed for the *trans*-[Ru(C≡CAr)Cl(dppe)$_2$] complexes (Scheme 3).[26] The synthesis of these tetra-substituted porphyrins featuring bis-alkynyl ruthenium endgroups was achieved in one pot, without attempt to isolate the intermediate vinylidene species, triethylamine being added to the reaction mixture together with the other reactants. The desired complexes **3**–X were obtained in good yields from **2** after ca. 72 h stirring at 40 °C. These new complexes were fully characterized by means of IR, UV and NMR (as example for **3**–X, for X=OMe, see Supplementary data; Fig. S2) spectroscopies, microanalyses, and CV. Attempts to detect the molecular ions of these species by ESI-MS or MALDI-MS were unsuccessful, but constituent fragments were observed in each case;[32] these complexes apparently undergo extensive fragmentation in the mass spectrometer.

While signals resembling those previously observed for **2** are detected in the ^{1}H and ^{13}C NMR spectra, additional signals corresponding to the presence of the terminal arylethynyl fragments in **3**–X are also observed, with the correct integrations, confirming the presence of the tetraruthenated porphyrin core. In particular, NMR is diagnostic of the high symmetry of the various compounds isolated, indicating that the chloride metathesis occurs at all of the Ru(II) centres of **2**. The unique singlet observed in the ^{31}P NMR spectrum is now located at ca. 54 ppm (Table 1). This shift to lower field relative to the same signal in **2** is diagnostic of the presence of the bis-alkynyl Ru(II) moieties in **3**–X.[30] As is often observed for bis-alkynyl Ru(II) complexes,[23] both $\nu_{C\equiv C}$ modes appear as a single and broad absorption at ca. 2050 cm^{-1} (Table 1). This characteristic vibration is shifted to slightly lower energies (2042 cm^{-1}) for the nitro compound **3**–NO_2 in comparison to the other **3**–X compounds,[33] which exhibit this broad $\nu_{C\equiv C}$ band at ca. 2056 cm^{-1}.[31] As seen previously with closely related bis-alkynyl Ru(II) compounds,[23] only one broad $\nu_{C\equiv C}$ band is observed for **3**–NO_2 in spite of the presence of two dissimilar alkynyl ligands at the Ru(II) centre.[29]

2.3. Cyclic voltammetry

Cyclic voltammetry (CV) studies were then performed in dichloromethane on **2** and on the **3**–X derivatives (Table 4). For **2**, a reversible electrochemical process corresponding to the simultaneous oxidation of the four organoruthenium(II) termini is observed at 0.48 V (Table 2). This value is not far removed from the value of 0.44 V observed for the corresponding chloridophenylalkynyl Ru(II) complex **6**–H (Scheme 4).[23] The comparatively higher oxidation potential indicates a slightly more difficult

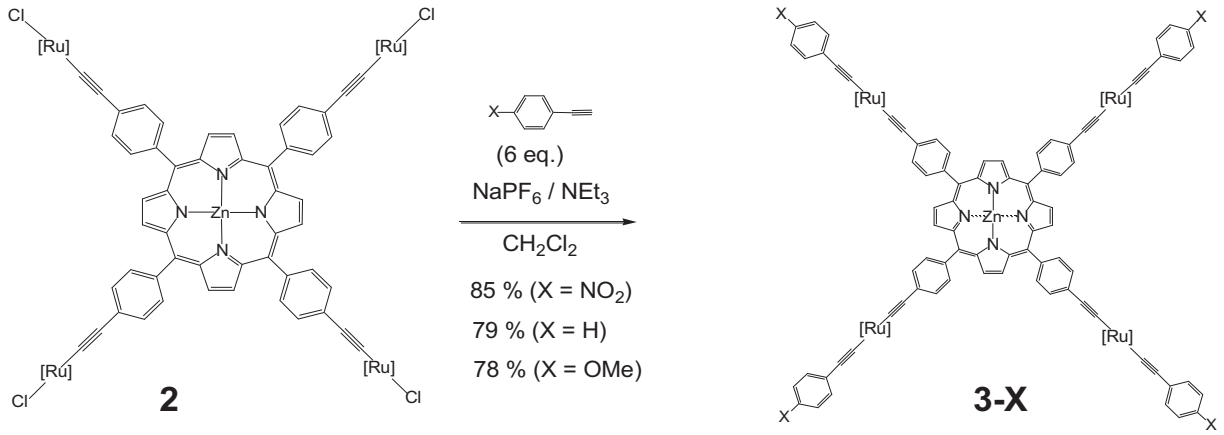

Scheme 3. Synthesis of the *trans*-substituted pentametallic porphyrins **3**–X (X=NO_2, H, OMe).

Table 2
Oxidation potentials for complexes **2**, **3**–X and **5**[a,b]

Compounds	$E^{\circ}_{Ru(III)/Ru(II)}$ (V)	$E^{\circ}_{ZnTPP/ZnTPP^{+}/ZnTPP^{2+}}$ (V)
2	0.49[c]	0.87, 1.16
3–NO_2	0.57[c]	0.86, 1.21
3–H	0.46[c]	0.88, 1.21
3–OMe	0.34[c]	0.84[d]
5	—	0.87, 1.14

[a] V versus SCE.
[b] Conditions: CH_2Cl_2, 0.1 M $[NBu_4][PF_6]$, scan rate 0.1 V s^{-1}.
[c] Fe(C≡CPh)(dppe)(η^5-C_5Me_5) was used as an internal calibrant $E^{\circ}_{Fe(III)/Fe(II)} = -0.15$ V versus SCE).[42]
[d] An irreversible oxidation occurs at 1.16 V.

undergoes two chemically reversible one-electron processes at ca. 0.92 V and 1.18 V versus SCE.[34] In addition, the voltammogram of the precursor porphyrin **5** (used to synthesize **2**) shows two pseudo-reversible oxidation waves at 0.87 V and 1.14 V versus SCE. The present data indicate that *para*-substitution of the porphyrin phenyl groups with ruthenium alkynyl moieties has only a weak effect on the oxidation of the porphyrin core. This observation is consistent with previous statements pertaining to substituent effects on the *meso*-aryl groups.[34,35] In the present system, the well known kinetic instability of Ru(III) alkynyl complexes in solution[36,37] may decrease somewhat the chemical reversibility of the porphyrin-centred oxidations at ambient temperatures.

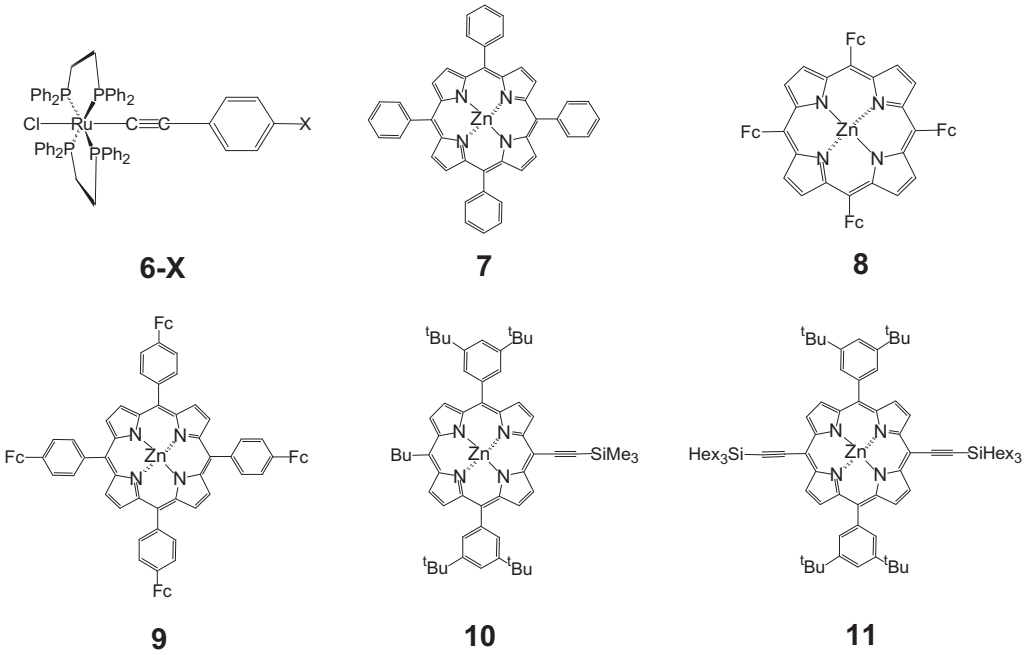

Scheme 4. Selected Ru(II) alkynyl complexes and porphyrins.

oxidation of the four Ru(II) centres in **2** than for the unique Ru(II) centre in **6**. The voltammogram of **2** shows two additional pseudo-reversible processes at 0.87 V and near 1.16 V versus SCE, but decreased in intensity by approximatively 25%. These redox waves are attributed to the stepwise one-electron oxidations of the metallated porphyrin macrocycle. Indeed, ZnTPP (**7**; Scheme 4) usually

For **3**–NO_2 and **3**–H compounds, similar voltammograms to **2** are obtained in the 0–1.3 V range, exhibiting three waves in a 4:1:1 ratio. The most intense process occurs at the lowest potential, again corresponding to the simultaneous oxidation of the Ru(II) centres, while the higher potential processes correspond to the first two oxidations of the ZnTPP-core. For **3**–OMe, an additional irreversible

process masks the second porphyrin-based oxidation, while for **3**–NO_2, another strong irreversible wave is observed at −0.96 V, which corresponds to the multi-electron reduction of the nitroaryl groups.[31,38,39]

In comparison to **2**, the Ru(III/II) potentials of **3**–H are slightly lower (0.46 V vs 0.49 V), as expected from the more electron-donating character of the arylalkynyl ligand relative to the chlorido ligand.[9] Within the **3**–X series, classic substituent effects control the Ru-centred oxidation potentials.[31,36] As expected, the potential is lowered for the compound **3**–OMe with four peripheral electron-donating methoxy groups, while the opposite is found for **3**–NO_2 with strongly electron-withdrawing nitro groups (Table 2). In contrast, the porphyrin-based oxidations appear only weakly affected by modifications in the trans-ligand at the peripheral ruthenium centres (Table 2).

A comparison to other symmetrically functionalized porphyrins bearing redox-active substituents on their periphery is also instructive. Thus, the Zn(II) porphyrin **8** (Scheme 4), which has four ferrocenyl groups appended to its *meso*-positions, exhibits several resolved Fc-based oxidations.[40] In the present system, the observation of a single wave for the oxidation of the peripheral organometallic substituents in **2** or **3**–X is indicative of a weaker electronic interaction between them, as was observed for **9** with the four ferrocenyl substituents on the *para*-positions of the *meso*-phenyl groups.[41] The observation of a chemically reversible and *simultaneous* oxidation of the four metal-alkynyl substituents in **2** or **3**–X is of interest in possible redox-switching of the NLO properties,[8,9,18] since this oxidation will preserve the symmetry of the compound, and thereby facilitate our analysis of the physics underlying the switching phenomenon.

2.4. UV–visible spectroscopy

The UV–visible absorption spectra of compounds **2** or **3**–X were recorded at room temperature in dichloromethane and compared to that of their tetra-ethynyl precursor **5** (Fig. 1). For **5**, the absorption spectrum shows the characteristic spectrum of a metallated porphyrin, with a Soret band at 425 nm and two Q bands at 552 and 594 nm.[22]

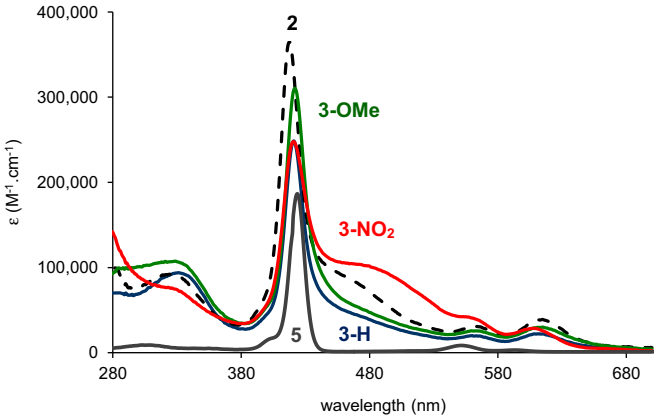

Fig. 1. UV–visible absorption spectra of the zinc porphyrins **2** and **3**–X (X=NO_2, H, OMe) in CH_2Cl_2 at 25 °C. For comparison, the compound **5** (with ε/values divided by 3) is also reported under the same conditions.

For **2** and the **3**–X derivatives, a slight hypsochromic shift of the Soret band is observed relative to **5** ($\Delta\nu$=167–395 cm^{-1}), while the two Q bands are bathochromically shifted (Table 3). No other absorption bands could be detected at longer wavelengths (until 2000 nm). Overall, the energies of the Soret and Q bands are only weakly influenced by a change in the terminal X-substituent. The weakness of their shifts within the **3**–X series is consistent with the porphyrin core experiencing only a weak influence of the peripheral electron-rich Ru(II) endgroups. It is noteworthy that a larger bathochromic shift ($\Delta\nu$=486 cm^{-1}) of the Soret band relative to **5** had been observed in earlier work (Scheme 1), upon complexation of platinum(II) to the terminal ethynyl groups,[22] suggesting a slightly different interaction between the porphyrin core and the peripheral metal-alkynyl fragments in **1** relative to **2** or **3**–X.

Table 3
UV–vis data for complexes **2**, **3**–X and **5**

Compounds	λ in nm (ε in 10^3 L mol^{-1} cm^{-1})
2	327 (93); 418 (364); 452 (sh, 97); 563 (31); 615 (39)
3–NO_2	322 (77); 420 (248); 466 (sh, 104); 553 (sh, 42); 607 (30)
3–H	330 (94); 421 (249); 460(sh, 50); 563 (20); 612 (39)
3–OMe	321 (107); 422 (310); 460 (sh, 61); 562 (26); 611 (30)
5	302 (27); 424 (556); 552 (28); 594 (10)

A new absorption band appears near 330 nm upon functionalization of the pendant ethynyl substituents of **5** by organoruthenium groups; this is a spectral region where $d_{Ru} \rightarrow \pi^*_{C\equiv C}$ transitions are often observed with Ru(II) alkynyl complexes.[9] Given that such an absorption is also observed for **4**, we tentatively propose that it corresponds to a $d_{Ru} \rightarrow \pi^*_{C\equiv CTPP}$ MLCT transition. Consistent with such an assignment, its energy across the **3**–X series seems poorly influenced by a change in the terminal arylalkynyl ligand. For these bis-alkynyl complexes, a second band corresponding to a $d_{Ru} \rightarrow \pi^*_{C\equiv C(4-C_6H_4X)}$ MLCT transition is also observed in the same spectral region,[9] except for **3**–NO_2, for which it appears as a shoulder on the Soret band, at 466 nm, due to its strong $d_{Ru} \rightarrow \pi^*_{NO_2}$ character. Such a transition is quite specific to *trans*-[Ru(dppe)$_2$] fragments with 4-nitroarylalkynyl ligands, and was previously observed at 484 nm for **6**–NO_2.[31]

2.5. Nonlinear absorption measurements

Standard femtosecond *Z*-scan measurements were then carried out on the various extended porphyrins **3**–X in dichloromethane (Fig. 2 (for X=H) and see Supplementary data; Fig. S1 (for X=OMe, NO_2); compound **2** proved insufficiently soluble for performing such measurements). Measurements were performed in the spectral range between 530 and 1600 nm, with simultaneous recording of the open- and closed-aperture signals. It should be emphasized that this region partly overlaps the one-photon absorptions of all the compounds (the Q bands) and so two-photon transitions to many states can be expected in this range, although it must be kept in mind that different selection rules govern one-photon and two-photon transitions. Due to the presence of various resonances, the NLO properties in the investigated wavelength range are likely to contain several contributions, including that of saturation of absorption (SA), so the NLO parameters need to be treated as 'effective' responses (as well as contributions from SA, the NLO parameters may be laser pulse width- and pulse energy-dependent). The *Z*-scan traces obtained from these studies were used to calculate the effective values of the real and imaginary parts of the cubic hyperpolarizability γ of the chromophores. However, the real parts of γ were found to exhibit complex behaviour which, together with inherently large errors in their determination (they are calculated from differences between scans for a solution and that for the solvent alone), has rendered it impossible to analyze them at the present stage. We therefore focus here on the absorptive nonlinearities, represented by the imaginary parts of γ, which were determined and subsequently converted into two-photon absorption cross-sections (σ_{2eff}) (Table 4). The data reveal that all **3**–X complexes behave as two-photon absorbers around 1100 and 710 nm. For the nitro- and methoxy-containing

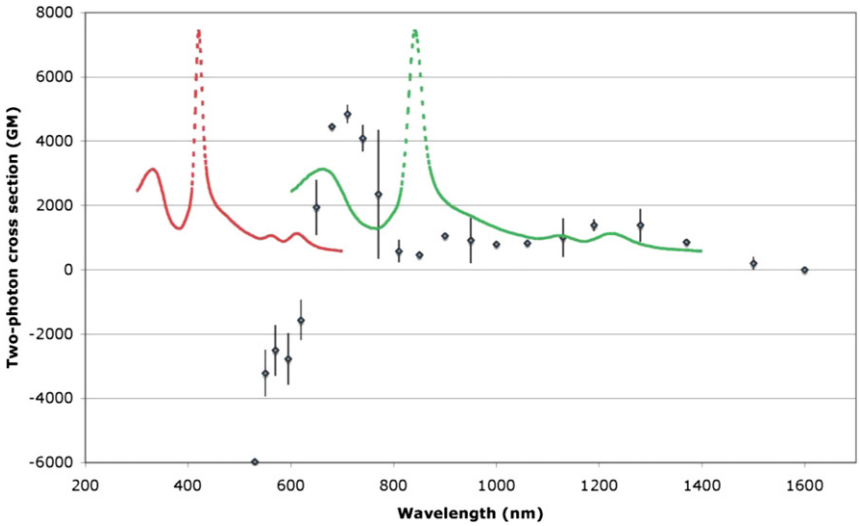

Fig. 2. Nonlinear absorption measurements represented as effective two-photon absorption cross-sections overlayed with the one-photon absorption (OPA) spectrum (red curve) and the same OPA spectrum plotted against twice the wavelength (green curve) for **3**–H.

Table 4
Comparison of extremal values of the effective two-photon absorption cross-sections (σ_{2eff}) for given wavelengths between 600 and 1600 nm for **3**–X complexes

Compound	σ_{2eff} (first max.) [GM]	λ (first max.) [nm]	σ_{2eff} (second max.) [GM]	λ (second max.) [nm]	σ_{2eff} (first min.) [GM]	λ (first min.) [nm]
3–NO_2[a]	6000±3000	770	1500±500	1000	−4500±200	620
3–H	4800±500	710	1400±500	1300	−2800±600	595
3–OMe[a]	4200±500	710	1300±100	1000	−1400±400	620

[a] An additional maximum is apparent at λ<530 nm with $\sigma_{2eff}\geq$6400 GM.

complexes, a third two-photon absorption (TPA) peak is found at higher energies, near 530 nm. In addition, all **3**–X complexes show SA behaviour near 600 nm, in a spectral range, which roughly corresponds to their second Q band.

The best TPA performances were obtained near 710 nm for **3**–NO_2 and **3**–H, with effective cross-sections exceeding 4500 GM. However, since these processes partly overlap with the SA process near 600 nm, the measured σ_{2eff} values result from a competition between these two processes, a situation that likely leads to an underestimation of the actual cross-section of the pure TPA process. Also, the presence of ultrafast reverse saturable absorption (RSA) processes that contributes to the effective TPA cross-sections near 710 nm found cannot be disregarded at this stage.[13] However, these appear unlikely due to the poor overlap with the second Q band. This must also be considered when attempting any comparison between the σ_{2eff} values near 710 nm for the different compounds.

Given the centrosymmetric nature of these molecules, selection rules predict that excited states to which transitions are allowed for one-photon processes should be forbidden for two-photon processes, and vice-versa.[12] Thus, examination of the OPA spectra is at best indicative of the nature of the excited state involved in the TPA process. The poor match between the OPA and TPA peaks suggests that none of the observed TPA bands can be ascribed to a reduction in symmetry due to the presence of conformers in solution. It is especially interesting that the one-photon Soret band near 400 nm does not have a two-photon analogue at ca. 800 nm; in contrast, there seems to be some antiresonant behaviour in this region. The small TPA peaks observed at ca. 1100 nm can be tentatively associated with excited states similar to those at the origin of the Q bands—their poor X-substituent dependency is consistent with such an assignment. The main TPA peaks near 710 nm roughly correspond to the onset of OPA peaks at ca. 350 nm (Fig. 2), perhaps suggestive of the involvement of a 'dark' MLCT state in this process. Consistent with such a hypothesis, a more pronounced dependence of the σ_{2eff} values on the nature of the X-substituent is suggested by the data (being mindful of the experimental error margins), the strongest effective cross-section being obtained for the most electron-withdrawing substituents. This is reminiscent of the fact that related 4-nitroarylalkynyl Ru(II) complexes are often found to present larger effective TPA cross-sections than their unsubstituted couterparts.[38,43] However, as mentioned above, the comparison between effective TPA cross-sections determined for **3**–X compounds must be undertaken with care due to the occurrence of an SA process in the same spectral range, as manifested by the presence of negative values for the effective cross-section around 600 nm.[13]

Finally, comparison with the literature data reveals that related porphyrins such as **10**[14] or **11**[15] (Scheme 4) possess very weak TPA (<50 GM) above 700 nm, behaviour that was also predicted by independent DFT calculations conducted on Zn(II) porphyrins modelling **11**. These calculations also suggested that, for **11**, a more efficient TPA process may occur at higher energy, just below 600 nm, and would originate from a dark porphyrin-based excited state with an energy just above that of the Soret band.[44] With **3**–X derivatives, similar states could be at the origin of the TPA peak detected near 700 nm. However, the effective cross-sections found for these compounds are much larger than the theoretical predictions for the porphyrin modelling **11**. Instead, as discussed above, we believe that the state at the origin of this two-photon absorption process corresponds to a $d_{Ru} \rightarrow \pi^*_{C\equiv C}$ MLCT state, in line with the slight substituent-dependency seen for the cross-sections.

3. Conclusions

We have synthesized and characterized four new centrosymmetric architectures **2** and **3**–X (X=NO_2, H, OMe) bearing four peripheral ethynyl groups from the known ZnTPP complex **5**. These new compounds were characterized by the usual spectroscopies and cyclic voltammetry. Both **2** and **3**–X compounds exhibit a chemically reversible oxidation at ca. 0.5 V versus SCE, which corresponds to the simultaneous oxidation of all the Ru(II) centres. Their electronic absorption spectra are dominated by a strong Soret band in the visible range, with a strong charge-transfer band also apparent as a shoulder in the case of **3**–NO_2. Preliminary studies of

the cubic NLO activity by *Z*-scan in the 500–1600 nm range for the **3**–X derivatives revealed that all of these organometallic porphyrins behave as strong two-photon absorbers at ca. 700 and 1100 nm, with effective TPA cross-sections significantly larger than those reported for related monomeric zinc porphyrin derivatives, although the participation of RSA processes near 710 nm cannot be definitively excluded yet. Their effective TPA characteristics exhibit no obvious dependencies on the terminal X-substituent, except perhaps for the TPA process at ca. 700 nm, for which slightly larger effective cross-sections were obtained for X=NO_2. All compounds possess substituent-dependent SA behaviour at ca. 600 nm, which appears strongly favoured with electron-withdrawing X-substituents. Ongoing studies are directed at identifying the excited states at the origin of these remarkable cubic NLO features, and at assessing the potential of these redox-active compounds for electro-switching their optical properties.

4. Experimental section

4.1. General procedures

All reactions were performed under argon with magnetic stirring. Solvents were distilled from appropriate drying agents prior to use: CH_2Cl_2 from CaH_2, $CHCl_3$ from P_2O_5 and all other solvents were HPLC grade. Commercially available reagents were used without further purification unless otherwise stated. All reactions were monitored by thin-layer chromatography (TLC) with Merck precoated aluminium foil sheets (Silica gel 60 with fluorescent indicator UV_{254}). Compounds were visualized with ultraviolet light at 254 and 365 nm. Column chromatography was carried out using silica gel from Merck (0.063–0.200 mm). ^{1}H NMR, ^{31}P and ^{13}C NMR in $CDCl_3$ were recorded using Bruker 200 DPX, 300 DPX and 500 DPX spectrometers. The chemical shifts are referenced to internal TMS. The assignments follow the numbering scheme shown in Scheme 5 and were obtained from 2D NMR experiments: COSY (Correlation Spectroscopy), HMBC (Heteronuclear Multiple Bond Correlation) and HMQC (Heteronuclear Multiple Quantum Coherence). IR spectra were recorded on a Bruker IFS 28 spectrometer using KBr pellets. UV–vis–NIR spectra were recorded on an UVIKON XL spectrometer from Biotek instruments. Cyclic voltammetry studies were performed in CH_2Cl_2 with a concentration of 0.1 M $[NBu_4][PF_6]$ as supporting electrolyte. Potentials reported were measured and are expressed relative to the saturated calomel electrode (SCE). High-resolution mass spectra were recorded on a ZabSpec TOF Micromass spectrometer in ESI positive mode in CH_2Cl_2/MeOH (95:5) at the CRMPO (Univ. Rennes 1). The *cis*-$[RuCl_2(dppe)_2]$ complex **3** was prepared according to literature methods.[26] The synthetic protocol used to obtain the known porphyrin **5**[22] is given in Supplementary data. The porphyrins were precipitated from a chloroform/heptane mixture.

4.2. Synthesis

*4.2.1. Zinc(II)-5,10,15,20-tetra{trans-(4-phenylethynyl)[ruthenium(II) bis(bis(1,2-(diphenylphosphino)ethane)](chloride)} (**2**).* $NaPF_6$ (95 mg, 0.57 mmol) was added to a solution of **5** (100 mg, 0.13 mmol) and *cis*-$[RuCl_2(dppe)_2]$ (**3**; 551 mg, 0.57 mmol) in CH_2Cl_2 (100 mL). This mixture was stirred at room temperature for 12 h and the solution was filtered. The compound was then precipitated by addition of Et_2O. The resulting precipitate was dissolved in CH_2Cl_2 and NEt_3 was added (1 mL) and the solution was stirred for a 10 additional minutes. The solution was concentrated and hexane was added, and the resulting precipitate was filtered and washed with MeOH (2×10 mL), to afford **2** as a green product (424 mg, 0.094 mmol). Yield: 73%. ^{1}H NMR (500 MHz, $CDCl_3$, δ in ppm): 9.22 (s, 8H, $H_{\beta\text{-pyrrolic}}$), 8.05 (d, 8H, $^3J_{H,H}$=8.2 Hz, H_b), 7.79 (m, 32H, $H_{para/Ar/dppe}$), 7.40–7.03 (m, 128H, $H_{ortho-meta/Ar/dppe}$), 7.13 (d, 8H, $^3J_{H,H}$=8.2 Hz, H_c), 2.85 (m, 32H, $CH_{2/dppe}$). ^{13}C NMR (125 MHz, $CDCl_3$, δ in ppm): 151.1 (s, $C_{\alpha\text{-pyrrolic}}$), 138.0 (s, $C_{Ar}[C_a]$), 137.6 and 136.3 (m, $C_{ipso/dppe}$), 135.3 and 135.2 (s, $CH_{Ar/dppe}$), 134.9 (s, $CH_{Ar}[C_b]$), 132.6 (s, $C_{\beta\text{-pyrrolic}}$), 130.2 (s, $C_{Ar}[C_d]$), 129.7 and 129.5 (s, $CH_{Ar/dppe}$), 128.9 (s, $CH_{Ar}[C_c]$), 128.1 and 127.7 (s, $CH_{Ar/dppe}$), 122.6 (s, C_{meso}), 114.8 (s, Ru*C*≡*C*[C_f]), 31.7 (m, $CH_{2/dppe}$); 1Ru*C*≡*C*[C_f] not observed, possibly overlapped. ^{31}P NMR (81 MHz, $CDCl_3$, δ in ppm): 51.0 (s, 16P, $(dppe)_2Ru$). Anal. Calcd for $C_{260}H_{216}Cl_4N_4P_{16}Ru_4Zn\cdot CHCl_3$: C, 67.81; H, 4.73; N, 1.21. Found: C, 67.84; H, 4.77; N 1.32. FTIR (ν, KBr, cm^{-1}): 2057 (vs, Ru*C*≡*C*). HRMS-ESI (*m*/*z*): calcd for $[C_{260}H_{216}Cl_4N_4P_{16}Ru_4Zn]^{2+}$: 2251.8556, found: 2251.8359 (Scheme 5).

*4.2.2. Zinc(II)-5,10,15,20-tetra{trans-(4-phenylethynyl)[ruthenium(II) bis(bis(1,2-diphenylphosphino)ethane)](4-nitrophenylethynyl)} (**3**–NO_2).* $NaPF_6$ (18 mg, 0.11 mmol) and NEt_3 (0.5 mL) were added

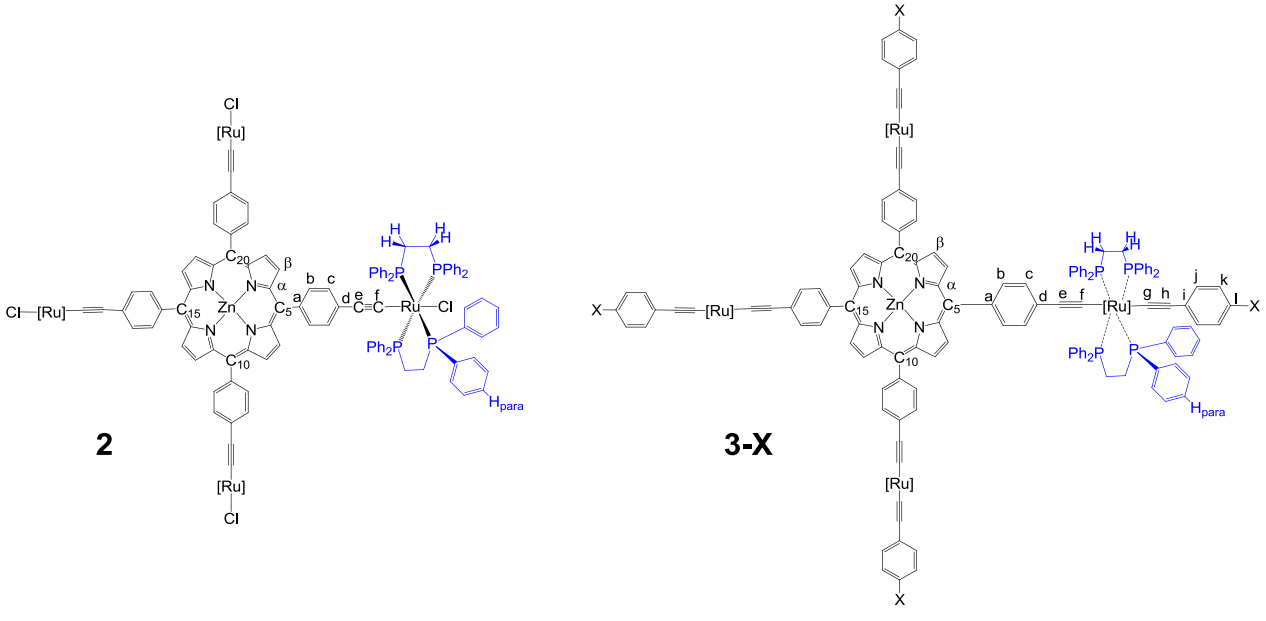

Scheme 5. Atomic numbering scheme for the labelling of the NMR spectra of **2** and **3**–X.

to a solution of **2** (70 mg, 0.015 mmol) and 1-ethynyl-4-nitrobenzene (10 mg, 0.060 mmol) in CH_2Cl_2 (10 mL). The mixture was then heated at reflux for 72 h and the reaction mixture was filtered. The compound was subsequently precipitated by addition of hexane to the filtrate and washed with MeOH (2×10 mL) to afford **3**–NO_2 as a green product (63 mg). Yield: 85%. ^{1}H NMR (500 MHz, $CDCl_3$, δ in ppm): 9.23 (s, 8H, $H_{\beta\text{-pyrrolic}}$), 8.13 (d, 8H, $^3J_{HH}$=7.6 Hz, H_b), 8.03 (d, 8H, $^3J_{H,H}$=8.5 Hz, H_k), 7.89 (m, 32H, $H_{para/Ar/dppe}$), 7.42 (m, 32H, $H_{Ar/dppe}$), 7.40–6.90 (m, 96H, $H_{Ar/dppe}$), 7.31 (d, 8H, $^3J_{H,H}$=8.1 Hz, H_c), 6.62 (d, 8H, $^3J_{H,H}$=8.4 Hz, H_j), 2.80 (m, 32H, $CH_{2/dppe}$). ^{13}C NMR (125 MHz, $CDCl_3$, δ in ppm): 150.9 (s, $C_{\alpha\text{-pyrrolic}}$), 143.1 (s, $C_{Ar}[C_l]$), 138.4 (s, $C_{Ar}[C_a]$), 138.1 (s, $C_{Ar}[C_i]$), 137.5, 137.1 (m, $C_{ipso/dppe}$), 135.0 and 134.4 (s, $CH_{Ar/dppe}$), 134.8 (s, $C_{Ar}[C_i]$), 132.6 (s, $C_{\beta\text{-pyrrolic}}$), 130.4 (s, $CH_{Ar}[C_j]$), 129.9 (s, $C_{Ar}[C_d]$), 129.6 and 129.5 (s, $CH_{Ar/dppe}$), 128.5 (s, $CH_{Ar}[C_c]$), 127.9 and 127.7 (s, $CH_{Ar/dppe}$), 123.9 (s, $CH_{Ar}[C_k]$), 122.3 (s, C_{meso}), 119.4 and 119.0 (s, RuC≡C[$C_{e/h}$]), 32.0 (m, $CH_{2/dppe}$); 2RuC≡C[$C_{f/g}$] not observed, possibly overlapped. ^{31}P NMR (81 MHz, $CDCl_3$, δ in ppm): 54.7 (s, 16P, $(dppe)_2Ru$). Anal. Calcd for $C_{292}H_{232}N_8O_8P_{16}Ru_4Zn\cdot 2CHCl_3$: C, 68.10; H, 4.55; N, 2.16. Found: C, 68.47; H, 4.56; N 2.25. FTIR (ν, KBr, cm^{-1}): 2042 (RuC≡C).

*4.2.3. Zinc(II)-5,10,15,20-tetra{trans-(4-phenylethynyl)[ruthenium(II) bis(bis(1,2-diphenylphosphino)ethane)](phenylethynyl)} (**3**–H).* $NaPF_6$ (35 mg, 0.21 mmol) and NEt_3 (0.5 mL) were added to a solution of **2** (60 mg, 0.013 mmol) and phenylacetylene (9 μL, 0.08 mmol) in CH_2Cl_2 (10 mL). The mixture was heated at reflux for 72 h and this reaction mixture was filtered. The compound was precipitated by addition of hexane to the filtrate and washed with MeOH (2×10 mL) to afford **3**–H as a green product (50 mg). Yield: 79%. ^{1}H NMR (500 MHz, $CDCl_3$, δ in ppm): 9.22 (s, 8H, $H_{\beta\text{-pyrrolic}}$), 8.12 (d, 8H, $^3J_{HH}$=8.1 Hz, H_b), 7.84 (m, 8H, $H_{Ar/dppe}$), 7.75 (m, 32H, $H_{para/Ar/dppe}$), 7.62 (m, 32H, $H_{Ar/dppe}$), 7.55–6.90 (m, 88H, $H_{Ar/dppe}$), 7.32 (t, 4H, $^3J_{H,H}$=7.3 Hz, H_l), 7.19 (d, 8H, $^3J_{H,H}$=7.3 Hz, H_c), 7.17 (d, 8H, $^3J_{H,H}$=7.2 Hz, H_k), 6.82 (d, 8H, $^3J_{H,H}$=7.1 Hz, H_j), 2.80 (m, 32H, $CH_{2/dppe}$). ^{13}C NMR (125 MHz, $CDCl_3$, δ in ppm): 151.1 (s, $C_{\alpha\text{-pyrrolic}}$), 137.9 (m, $C_{ipso/dppe}$), 135.2 and 135.1 (s, $CH_{Ar/dppe}$+$CH_{Ar}[C_b]$), 132.6 (s, $C_{\beta\text{-pyrrolic}}$), 131.4 (s, $C_{Ar}[C_a]$), 130.7 (s, $CH_{Ar}[C_j]$), 130.4 ($C_{Ar}[C_d]$), 129.5 and 129.3 (s, $CH_{Ar/dppe}$+$CH_{Ar}[C_c]$), 128.9 (s, $C_{Ar}[C_i]$), 128.1 (s, $CH_{Ar}[C_k]$), 127.9 and 127.8 (s, $CH_{Ar/dppe}$), 123.6 (C_l, $CH_{Ar}[C_l]$), 122.6 (s, C_{meso}), 117.6 and 117.5 (s, RuC≡C[$C_{e/h}$]), 32.3 (m, $CH_{2/dppe}$); 2RuC≡C[$C_{f/g}$] not observed, possibly overlapped. ^{31}P NMR (81 MHz, $CDCl_3$, δ in ppm): 55.2 (s, 16P, $(dppe)_2Ru$). Anal. Calcd for $C_{292}H_{236}N_4P_{16}Ru_4Zn\cdot 2CHCl_3$: C, 70.55; H, 4.79; N, 1.12. Found: C, 70.83; H, 5.04; N 1.33. FTIR (ν, KBr, cm^{-1}): 2056 (RuC≡C).

*4.2.4. Zinc(II)-5,10,15,20-tetra{trans-(4-phenylethynyl)[ruthenium(II) bis(bis(1,2-diphenylphosphino)ethane)](4-methoxyphenylethynyl)} (**3**–OMe).* $NaPF_6$ (24 mg, 0.13 mmol) and NEt_3 (0.5 mL) were added to a solution of **2** (70 mg, 0.015 mmol) and 1-ethynyl-4-methoxybenzene (12 mg, 0.094 mmol) in CH_2Cl_2 (10 mL). The mixture was heated at reflux for 72 h and the reaction mixture was filtered. The compound was then precipitated by addition of hexane and washed with MeOH (2×10 mL) to afford **3**–OMe as a green product (60 mg). Yield: 78%. ^{1}H NMR (500 MHz, $CDCl_3$, δ in ppm): 9.23 (s, 8H, $H_{\beta\text{-pyrrolic}}$), 8.09 (d, 8H, $^3J_{H,H}$=8.1 Hz, H_b), 7.84 (m, 8H, $H_{Ar/dppe}$), 7.75 (m, 32H, $H_{Ar/dppe}$), 7.64 (m, 32H, $H_{Ar/dppe}$), 7.60–6.95 (m, 88H, $H_{Ar/dppe}$), 7.19 (d, 8H, $^3J_{H,H}$=7.6 Hz, H_c), 6.78 (m, 16H, H_{j+k}), 3.86 (s, 12H, OCH_3), 2.79 (m, 32H, $CH_{2/dppe}$). ^{13}C NMR (125 MHz, $CDCl_3$, δ in ppm): 156.3 (s, $C_{Ar}[C_l]$), 150.9 ($C_{\alpha\text{-pyrrolic}}$), 137.9 (m, $C_{ipso/dppe}$), 135.0 and 134.9 (s, $CH_{Ar/dppe}$), 134.7 (s, $CH_{Ar}[C_b]$), 132.4 (s, $C_{\beta\text{-pyrrolic}}$), 131.4 (s, $CH_{Ar}[C_j]$), 130.3 (s, $C_{Ar}[C_d]$), 129.2 and 129.1 (s, $CH_{Ar/dppe}$), 128.6 (s, $CH_{Ar}[C_c]$), 127.7 and 127.5 (s, $CH_{Ar/dppe}$), 124.3 (s, $C_{Ar}[C_i]$), 122.4 (s, C_{meso}), 117.3 and 116.2 (s, RuC≡C[$C_{e/h}$]), 113.6 (s, $CH_{Ar}[C_k]$), 55.7 (s, OCH_3), 32.1 (m, $CH_{2/dppe}$); 2RuC≡C[$C_{f/g}$] and C_a not observed, possibly overlapped. ^{31}P NMR (81 MHz, $CDCl_3$, δ in ppm): 55.1 (s, 16P, $(dppe)_2Ru$). Anal. Calcd for $C_{296}H_{244}N_4O_4P_{16}Ru_4Zn\cdot 7CHCl_3$: C, 63.60; H, 4.42; N, 0.98. Found: C, 63.98; H, 4.64; N 1.31. FTIR (ν, KBr, cm^{-1}): 2056 (RuC≡C).

4.3. *Z*-scan measurements

Third-order nonlinear optical properties were investigated with an amplified femtosecond laser system using a Clark-MXR CPA-2001 Ti-sapphire regenerative amplifier to pump a Light Conversion TOPAS optical parametric amplifier. Experiments were performed in a wide range of wavelengths using different modes of the OPA output and employing polarizing optics, spatial filtering and colour glass filters to reject unwanted wavelengths. The pulse duration was approximately 150 fs and the repetition rate was 250 Hz. The pulse energy was adjusted to keep the nonlinear phase shifts that were obtained from the samples in the range of roughly 0.3–1.5 rad, which typically corresponded to light intensities of the order of 100 GW/cm.[2] Solutions of the compounds in dichloromethane of ca. 0.5 w/w % concentration were placed in 1 mm stoppered Starna glass cells. An identical cell was used for measurements of *Z*-scans on pure solvent. All measurements were calibrated by referencing to signals obtained from a 3 mm thick fused silica plate, and the NLO properties of the solute were determined as described previously.[38,45]

Acknowledgements

The 'Université Européenne de Bretagne' (UEB), FEDER, and RTR BRESMAT are acknowledged for an EPT grant, and the CNRS (PICS program N° 5676) is acknowledged for financial support. S.D. thanks the 'Ministère National de la Recherche et de la Technologie' (MNERT), A.M. thanks the 'Region Bretagne' and D.Y. thanks the China Scholarship Council (CSC) for their Ph.D. grants. M.S., K.M., J.O.-B. and M.W. were supported by the Foundation for Polish Science Welcome grant and by a statutory activity subsidy from the Polish Ministry of Science and Higher Education for the Faculty of Chemistry of WUT. M.G.H. and M.P.C. thank the Australian Research Council for support, an ARC Australian Professorial Fellowship (M.G.H.) and an ARC Australian Research Fellowship (M.P.C.). The authors are grateful to M.S. Jennaway (RSC, ANU) for technical support and S. Sinbandhit (CRMPO) for technical assistance and helpful discussions.

Supplementary data

Supplementary data associated with this article can be found in the online version, at http://dx.doi.org/10.1016/j.tet.2012.09.108.

References and notes

1. Marder, S. R. *Chem. Commun.* **2006**, 131–134.
2. Brédas, J. L.; Adant, C.; Tackx, P.; Persoons, A. *Chem. Rev.* **1994**, *94*, 243–278; He, G. S.; Tan, L. S.; Zheng, Q.; Prasad, P. N. *Chem. Rev.* **2008**, *108*, 1245–1330.
3. Prasad, P. N.; Williams, D. J. *Introduction to Nonlinear Optical Effects in Molecules and Polymers*; John Wiley & Sons: New York, NY, 1991; Luther-Davies, B.; Samoc, M. *Curr. Opin. Solid State Mater. Sci.* **1997**, *2*, 213–219; Samoc, M. *J. Mol. Model.* **2011**, *17*, 2183–2189.
4. di Bella, S.; Dragonetti, C.; Pizzotti, M.; Roberto, D.; Tessore, F.; Ugo, R. *Top. Organomet. Chem.* **2010**, *28*, 1–55; Maury, O.; Le Bozec, H. *Acc. Chem. Res.* **2005**, *38*, 691–703.
5. Morrall, J. P.; Dalton, G. T.; Humphrey, M. G.; Samoc, M. *Adv. Organomet. Chem.* **2008**, *55*, 61–136.
6. Humphrey, M. G.; Cifuentes, M. P.; Samoc, M. *Top. Organomet. Chem.* **2011**, *28*, 57–73.
7. Schwich, T.; Cifuentes, M. P.; Gugger, P. A.; Samoc, M.; Humphrey, M. G. *Adv. Mater.* **2011**, *23*, 1433–1435; Trujillo, A.; Veillard, R.; Argouarch, G.; Roisnel, T.; Singh, A.; Ledoux, I.; Paul, F. *Dalton Trans.* **2012**, *41*, 7454–7456.
8. Cifuentes, M. P.; Powell, C. E.; Humphrey, M. G.; Heath, G. A.; Samoc, M.; Luther-Davies, B. *J. Phys. Chem. A* **2001**, *105*, 9625–9627.
9. Powell, C. E.; Cifuentes, M. P.; Morrall, J. P.; Stranger, R.; Humphrey, M. G.; Samoc, M.; Luther-Davies, B.; Heath, G. A. *J. Am. Chem. Soc.* **2003**, *125*, 602–610.

10. Pawlicki, M.; Collins, H. A.; Denning, R. G.; Anderson, H. L. *Angew. Chem., Int. Ed.* **2009**, *48*, 3244–3266.
11. Ravikanth, M.; Ravindra, K. G. *Curr. Sci.* **1995**, *68*, 1010–1017.
12. de la Torre, G.; Vazquez, P.; Agullo-Lopez, F.; Torres, T. *Chem. Rev.* **2004**, *104*, 3723–3750.
13. Rao, S. V.; Srinivas, N. K. M. N.; Rao, D. N.; Giribabu, L.; Mayia, B. G.; Philip, R.; Kumar, G. R. *Opt. Commun.* **2000**, *182*, 255–264.
14. Odom, S. A.; Webster, S.; Padilha, L. A.; Peceli, D.; Hu, H.; Nootz, G.; Chung, S.-J.; Ohira, S.; Matichak, J. D.; Przhonska, O. V.; Kachkovski, A. D.; Barlow, S.; Brédas, J.-L.; Anderson, H. L.; Hagan, D. J.; Van Stryland, E. W.; Marder, S. R. *J. Am. Chem. Soc.* **2009**, *131*, 7510–7511.
15. Drobizhev, M.; Stepanenko, Y.; Dzenis, Y.; Karotki, A.; Rebane, A.; Taylor, P. N.; Anderson, H. L. *J. Am. Chem. Soc.* **2004**, *126*, 15352–15353; Drobizhev, M.; Stepanenko, Y.; Dzenis, Y.; Karotki, A.; Rebane, A.; Taylor, P. N.; Anderson, H. L. *J. Phys. Chem. B* **2005**, *109*, 7223–7236; Karotki, A.; Drobizhev, M.; Dzenis, Y.; Taylor, P. N.; Anderson, H. L.; Rebane, A. *Phys. Chem. Chem. Phys.* **2004**, *6*, 7–10.
16. Humphrey, J. L.; Kuciauskas, D. *J. Phys. Chem. C* **2006**, *128*, 3902–3903; Humphrey, J. L.; Kuciauskas, D. *J. Phys. Chem. B* **2004**, *108*, 12016–12023.
17. Rao, D. V. G. L. N.; Aranda, F. J.; Roach, J. F.; Remy, D. E. *Appl. Phys. Lett.* **1991**, *58*, 1241–1243.
18. Gauthier, N.; Argouarch, G.; Paul, F.; Toupet, L.; Ladjarafi, A.; Costuas, K.; Halet, J.-F.; Samoc, M.; Cifuentes, M. P.; Corkery, T. C.; Humphrey, M. G. *Chem.—Eur. J.* **2011**, *17*, 5561–5577 and refs therein.
19. Paul-Roth, C. O.; Rault-Berthelot, J.; Simonneaux, G. *Tetrahedron* **2004**, *60*, 12169–12175; Paul-Roth, C. O.; Rault-Berthelot, J.; Letessier, J.; Simonneaux, G.; Bergamini, J.-F. *J. Electroanal. Chem.* **2007**, *606*, 103–116.
20. Paul-Roth, C. O.; Simonneaux, G. *Tetrahedron Lett.* **2006**, *47*, 3275–3278; Paul-Roth, C. O.; Simonneaux, G. *C. R. Acad. Sci., Ser. IIb: Chim.* **2006**, *9*, 1277–1286; Paul-Roth, C. O.; Williams, J. A. G.; Letessier, J.; Simonneaux, G. *Tetrahedron Lett.* **2007**, *48*, 4317–4322; Drouet, S.; Paul-Roth, C. O.; Fattori, V.; Cocchi, M.; Williams, J. A. G. *New J. Chem.* **2011**, *35*, 438–444; Drouet, S.; Paul-Roth, C. O. *Tetrahedron* **2009**, *65*, 10693–10700; Drouet, S.; Merhi, A.; Argouarch, G.; Paul, F.; Mongin, O.; Blanchard-Desce, M.; Paul-Roth, C. O. *Tetrahedron* **2012**, *68*, 98–105.
21. Bellows, D.; Ali, S. M.; Gros, C. P.; Ojaimi, M. E.; Barbe, J.-M.; Guillard, R.; Harvey, P. D. *Inorg. Chem.* **2009**, *48*, 7613–7629; Chen, Y.-J.; Chen, S.-S.; Lo, S.-S.; Huang, T.-H.; Wu, C.-C.; Lee, G.-H.; Peng, S.-M.; Yeh, C.-Y. *Chem. Commun.* **2006**, 1015–1017.
22. Onitsuka, K.; Kitajima, H.; Fujimoto, M.; Iuchi, A.; Takei, F.; Takahashi, S. *Chem. Commun.* **2002**, 2576–2577.
23. Gauthier, N.; Olivier, C.; Rigaut, S.; Touchard, D.; Roisnel, T.; Humphrey, M. G.; Paul, F. *Organometallics* **2008**, *27*, 1063–1072.
24. See, for instance: Hurst, S. K.; Cifuentes, M. P.; Humphrey, M. G. *Organometallics* **2002**, *21*, 2353–2355.
25. Fox, M. A.; Harris, J. E.; Heider, S.; Pérez-Gregorio, V.; Zakrzewska, M. E.; Farmer, J. D.; Yufit, D. S.; Howard, J. A. K.; Low, P. J. *J. Organomet. Chem.* **2009**, *694*, 2350–2358.
26. Green, K. A.; Cifuentes, M. P.; Corkery, T. C.; Samoc, M.; Humphrey, M. G. *Angew. Chem., Int. Ed.* **2009**, *48*, 7867–7870.
27. Bonnet, J. J.; Eaton, S. S.; Eaton, G. R.; Holm, R. H.; Ibers, J. A. *J. Am. Chem. Soc.* **1973**, *95*, 2141–2149.
28. Lindsey, J. S.; Hsu, H. C.; Schreiman, I. C. *Tetrahedron Lett.* **1986**, *27*, 4969–4970.
29. Touchard, D.; Haquette, P.; Guesmi, S.; Le Pichon, L.; Daridor, A.; Toupet, L.; Dixneuf, P. H. *Organometallics* **1997**, *16*, 3640–3648.
30. McDonagh, A. M.; Powell, C. E.; Morrall, J. P.; Cifuentes, M. P.; Humphrey, M. G. *Organometallics* **2003**, *22*, 1402–1413.
31. Gauthier, N.; Tchouar, N.; Justaud, F.; Argouarch, G.; Cifuentes, M. P.; Toupet, L.; Touchard, D.; Halet, J.-F.; Rigaut, S.; Humphrey, M. G.; Costuas, K.; Paul, F. *Organometallics* **2009**, *28*, 2253–2266.
32. For other reports concerning the failure to characterize related compounds by MS, see Ref. 22.
33. Paul, F.; Mevellec, J.-Y.; Lapinte, C. *J. Chem. Soc., Dalton Trans.* **2002**, 1783–1790.
34. Paul-Roth, C. O.; Rault-Berthelot, J.; Simonneaux, G.; Pohriel, C.; Abdalilah, M.; Letessier, J. *J. Electroanal. Chem.* **2006**, *597*, 19–27.
35. Note that at the potential leading to the first oxidation of the porphyrin core, ruthenium centres are under their oxidized Ru(III) state, and so are far less electron-releasing than under their Ru(II) state.[31]
36. Paul, F.; Ellis, B. J.; Bruce, M. I.; Toupet, L.; Roisnel, T.; Costuas, K.; Halet, J.-F.; Lapinte, C. *Organometallics* **2006**, *25*, 649–665.
37. Bruce, M. I.; Burgun, A.; Gendron, F.; Grelaud, G.; Halet, J.-F.; Skelton, B. W. *Organometallics* **2011**, *30*, 2861–2868.
38. Babgi, B.; Rigamonti, L.; Cifuentes, M. P.; Corkery, T. C.; Randles, M. D.; Schwich, T.; Petrie, S.; Stranger, R.; Teshome, A.; Asselberghs, I.; Clays, K.; Samoc, M.; Humphrey, M. G. *J. Am. Chem. Soc.* **2009**, *131*, 10293–10307.
39. Dalton, G. T.; Cifuentes, M. P.; Watson, L. A.; Petrie, S.; Stranger, R.; Samoc, M.; Humphrey, M. G. *Inorg. Chem.* **2009**, *48*, 6534–6547.
40. Rohde, G. T.; Sabin, J. R.; Barrett, C. D.; Nemykin, V. N. *New J. Chem.* **2011**, *35*, 1440–1448.
41. Schmidt, E. S.; Calderwood, T. S.; Bruice, T. C. *Inorg. Chem.* **1986**, *25*, 3718–3720.
42. Denis, R.; Toupet, L.; Paul, F.; Lapinte, C. *Organometallics* **2000**, *19*, 4240–4251.
43. Cifuentes, M. P.; Powell, C. E.; Morrall, J. P. L.; McDonagh, A. M.; Lucas, N. T.; Humphrey, M. G.; Samoc, M.; Houbrechts, S.; Asselberghs, I.; Clays, K.; Persoons, A.; Isoshima, T. *J. Am. Chem. Soc.* **2006**, *128*, 10819–10832.
44. Zhou, X.; Ren, A.-M.; Feng, J.-K.; Liu, X.-J.; Zhang, Y.-D. *ChemPhysChem* **2004**, *4*, 991–997.
45. Samoc, M.; Samoc, A.; Dalton, G. T.; Cifuentes, M. P.; Humphrey, M. G.; Fleitz, P. A. Two-photon Absorption Spectra and Dispersion of the Complex Cubic Hyperpolarizability γ in Organic and Organometallic Chromophores In *Multiphoton Processes in Organics and their Application*; Rau, I., Kajzar, F., Eds.; Old City: Philadelphia, PA, 2011; pp 341–355.